

Structural, thermal and dissolution properties of MgO and CaO containing borophosphate glasses: Effect of Fe₂O₃ addition

Chao Tan^{abcd}, Ifty Ahmed^d, Andrew J. Parsons^d, Nusrat Sharmin^{bc}, Chenkai Zhu^{bc}, Jinsong Liu^e, Chris D. Rudd^{bcd} and Xiaoling Liu^{bc*}

- a. International Doctoral Innovation Centre, The University of Nottingham Ningbo China, Ningbo, 315100, China
- b. Ningbo Nottingham International Academy for the Marine Economy and Technology, The University of Nottingham Ningbo China, Ningbo, 315100, China
- c. Ningbo Nottingham New Materials Institute, The University of Nottingham Ningbo China, Ningbo, 315100, China
- d. Advanced Materials Research Group, Faculty of Engineering, The University of Nottingham, Nottingham, NG7 2RD, U.K.
- e. Department of Technology, Sinoma Co., Ltd., 198 Tongtian Road, Nanjing, 211100, China

* Corresponding author at Science and Engineering Building, the University of Nottingham Ningbo China, Ningbo, 315100, China. Tel: +86 (0)574 8818 2753, Email: Xiaoling.Liu@nottingham.edu.cn

Abstract

This paper investigated manufacture of high durability phosphate glass fibres for biomedical applications. Five different borophosphate glass formulations in the systems of 45P₂O₅-5B₂O₃-5Na₂O-(29-x)CaO-16MgO-(x)Fe₂O₃ and 45P₂O₅-5B₂O₃-5Na₂O-24CaO-(21-x)MgO-(x)Fe₂O₃ where x = 5, 8 and 11 mol% were produced via melt-quenching. The compositions and amorphous nature of the glasses were confirmed by ICP-MS and XRD, respectively. FTIR results indicated depolymerisation of the phosphate chains with a decrease in Q² units with increasing Fe₂O₃ content. DSC analyses showed an increase in T_g by ~5 °C with an increment of 3 mol% in Fe₂O₃ content. The thermal properties were also used to calculate processing window (i.e. T_{c,ons} - T_g) and another parameter, K_{gl}, to determine the suitability for fibre drawing directly from melt, which equals (T_{c,ons} - T_g)/(T_l - T_{c,ons}). The degradation study conducted in PBS solution at 37 °C showed a decrease of 25%-47% in degradation rate with increasing Fe₂O₃ content. This confirmed that the chemical durability of the glasses had increased, which was suggested to be due to Fe₂O₃ addition. Furthermore, the density measured via Archimedes method revealed a linear increase with increasing Fe₂O₃ content.

Keywords: Borophosphate glass; glass structure; thermal properties; glass stability; degradation.

Acknowledgements

This work was carried out at the International Doctoral Innovation Centre (IDIC). The authors acknowledge the financial support from Ningbo Education Bureau, Ningbo Science and Technology Bureau, China's MoST and The University of Nottingham. The work is also partially supported by EPSRC (Grant no. EP/L016362/1).

1. Introduction

Phosphate-based glasses (PBGs) have been studied as novel biomaterials for bone repair implants due to their chemical similarity to bone mineral [1, 2]. These glasses have also been produced in the form of fibres to reinforce absorbable polymers (like PLA and PCL) [1, 3-5]. Much work so far has focused on the PBGs containing 40-55 mol% P_2O_5 content for these applications, since a lower phosphate content has been shown to not be suitable for continuous glass fibre drawing [6], whilst a higher level would significantly decrease the chemical durability of the glass [5]. For instance, Ahmed et al. [2, 6] studied PBGs in the P_2O_5 -CaO- Na_2O system and reported the feasibility of fibre-drawing from glasses containing 50 and 55 mol% P_2O_5 . However, they found it was extremely difficult to manufacture fibres from fixed 45 mol% P_2O_5 ternary compositions. They suggested that long phosphate chain lengths facilitated the fibre drawing process as compared to shorter phosphate chain length compositions. However, follow-on studies [4] showed successful manufacture of continuous fibres from borophosphate glasses with fixed 45 mol% P_2O_5 . These studies also confirmed manufacture of continuous fibres from lower fixed 40 mol% P_2O_5 compositions with addition of 5-10 mol% B_2O_3 to the glasses, which was attributed to the lengthening of phosphate chains with addition of boron [7]. However, formulations with higher B_2O_3 addition were shown to decrease the biocompatibility of the phosphate glasses, which was suggested to be due to excessively release of boron ions [8, 9].

Adding iron oxide to PBGs has been shown to efficiently enhance their chemical durability, which in turn showed improvement in the biocompatibility of the glasses [10-14], due to the replacement of P-O-P bonds by Fe-O-P and stronger cross-linking between phosphate chains [15]. Furthermore, the stronger ionic cross-linking could also reduce the tendency of crystallisation in PBGs [5], which is an important factor when drawing fibres [16].

Considerable research has been devoted to CaO and/or MgO containing PBGs, in which the calcium and magnesium worked as glass network modifiers [17-20]. It has been hypothesised that MgO would make only a small difference in glass behaviour when compared to CaO due to their similar cation valence, however, it was also noteworthy that

MgO addition may cause an anomalous effect on the physical properties of the glasses with an abrupt coordination change in Mg^{2+} ions [21]. For instance, Sahar et al. [22] investigated binary MgO- P_2O_5 glass and observed an unusual discontinuity in their composition/property behaviour near the metaphosphate composition. Hoppe et al. [23] also found a coordination change in the ultra- to metaphosphate composition range of the MgO- P_2O_5 glass. However, explanation of the “phosphate anomaly” by a coordination change of the Mg^{2+} cation may no longer remain valid in more complex glass systems with very low MgO contents.

In order to produce high durability phosphate glass fibres, the effects of iron oxide addition (5-11 mol%) were investigated at the expense of calcium and magnesium, with fixed P_2O_5 , B_2O_3 and Na_2O contents at 45, 5 and 5 mol% respectively. It was expected that the presence of boron would improve the fibre drawing characteristics of the glass and that iron would significantly increase the chemical durability of the glass without adversely affecting the fibre drawing performance. Moreover, the CaO/MgO ratio was expected to have a minimal influence on the properties of the glass since the phosphate content was fixed.

During the study, the composition and structure of the glasses produced were investigated using ICP-MS, XRD and FTIR. The thermal properties were studied using DSC and TMA. Additionally, the density of the glasses was measured using an Archimedes method. The degradation study of the glasses was conducted in phosphate buffer saline (PBS) solution at 37 °C.

2. Materials and Methods

2.1. Glass production

The glasses were produced via a melt-quenching method. Five different glass compositions (see Table 1) were prepared using phosphorus pentoxide (P_2O_5), boric anhydride (B_2O_3), sodium phosphate monobasic (NaH_2PO_4), calcium phosphate dibasic ($CaHPO_4$), magnesium phosphate dibasic trihydrate ($MgHPO_4 \cdot 3H_2O$) and iron (III) phosphate dihydrate ($FePO_4 \cdot 2H_2O$) (Sigma Aldrich, UK) as starting materials. The precursors were mixed together and transferred to a 200 mL volume Pt/5%Au crucible (Birmingham Metal Company, UK), which was then placed into a furnace (preheated to 350 °C) for half an hour to evaporate water in the batch. The salt mixtures were subsequently melted in a furnace at 1200 °C for 1.5 hours. The molten glass was poured onto a steel plate and left to cool, or cast to Ø10 mm rods in a graphite mould preheated to 450 °C. The rods were then annealed for 1.5 hours at a

temperature of $T_g + 10$ °C, where T_g is the glass transition temperature as measured via differential scanning calorimetry (DSC).

Table 1 Glass formulations investigated in this study, in mol%.

Sample codes		P ₂ O ₅	B ₂ O ₃	Na ₂ O	CaO	MgO	Fe ₂ O ₃
Ca(29-x)Mg16Fe(x)	Ca24Mg16Fe5	45	5	5	24	16	5
	Ca21Mg16Fe8	45	5	5	21	16	8
	Ca18Mg16Fe11	45	5	5	18	16	11
Ca24Mg(21-x)Fe(x)	Ca24Mg16Fe5	45	5	5	24	16	5
	Ca24Mg13Fe8	45	5	5	24	13	8
	Ca24Mg10Fe11	45	5	5	24	10	11

2.2. Compositional analysis

Inductively coupled plasma mass spectrometry (ICP-MS, Thermo Scientific iCAP Qc, UK) was used to confirm the composition of the glass samples. The calibration of the instrument was conducted using the standard solutions containing B, P, Na⁺, Ca²⁺, Mg²⁺ and Fe³⁺ (Thermo Scientific, UK) at the concentrations of 20, 40 and 100 ppm in 2% HNO₃ in DI water. Standard sample concentrations were measured periodically to ensure the accuracy of the calibration curves. After calibrating, 0.2 g fine powder of each sample was digested in 50 mL 37% HCl to obtain a clear solution. Then 2.5 mL of the solution was diluted with 2.5 mL Milli-Q water and 45 mL 2% HNO₃. Following that, the diluted solution was filtered using a mesh of 0.2 µm prior to ICP-MS analysis. A blank run was performed for the baseline. Then the investigated solutions were ionised by electron impact and the ion current data for a specific m/Z (the mass-to-charge ratio) species was analysed.

2.3. Powder X-ray diffraction analysis

X-ray diffraction (XRD) scanning was used to confirm the amorphous nature of the glass samples. It was performed on a D500 diffractometer (Siemens) using CuKα radiation ($\lambda = 0.153$ nm), operating at a voltage of 40 kV and current of 25 mA with a step size of 0.05° and dwell time of 2 s from 10 to 100°. The result was analysed by DIFFRACplus software.

2.4. Fourier transform infrared spectroscopic analysis

A Bruker Vertex 70 FT-IR spectrometer was used for structural analysis of the glass samples. The using samples were prepared as pellets by pressing a mixture of glass powder (3 mg) and anhydrous KBr powder (200 mg). The infrared

(IR) spectrum was measured between 400 and 4000 cm^{-1} with the scan resolution of 4 cm^{-1} for 16 scans under purged dry air. The background of the spectrum was corrected with pure KBr.

2.5. Thermal analysis

Thermal traces were obtained using a differential scanning calorimeter (DSC, TA Instruments SDT Q600, UK). In the process, ~30 mg sample powder in a platinum pan was heated from room temperature to 560 $^{\circ}\text{C}$ at a heating rate of 20 $^{\circ}\text{C min}^{-1}$ in flowing argon gas [24]. A blank run was performed for the baseline. The glass transition temperature (T_g) was extrapolated from the intersection of the two tangents at the start of the corresponding endotherm of heat flow [25].

The samples were subjected to a heating cycle using the obtained T_g for a consistent thermal history [26]. Therefore, each sample was heated from room temperature to $T_g + 20$ $^{\circ}\text{C}$ at a rate of 20 $^{\circ}\text{C min}^{-1}$, held there isothermally for 15 min, and then cooled down at a rate of 10 $^{\circ}\text{C min}^{-1}$ to 50 $^{\circ}\text{C}$ before ramping up again to 1100 $^{\circ}\text{C}$ at a rate of 20 $^{\circ}\text{C min}^{-1}$ under argon gas. Afterwards, the glass transition temperature (T_g), the onset of crystallisation temperature ($T_{c,ons}$), the peak crystallisation temperature (T_c), the melting temperature (T_m) and the liquidus temperature (T_l) were determined for all the samples. Wherein the $T_{c,ons}$ was taken as the temperature at which the heat flow curve first deviated from the baseline prior to the first crystallisation peak above T_g [27] and the T_l was taken as the temperature at which the heat flow curve deviated from the last melting peak to the baseline.

Glass stability is defined in terms of resistance to crystallisation of a glass during heating and it is most important during processes involving reforming of an existing glass [28]. The super cooled liquid region, $T_{c,ons} - T_g$, (also called the processing window, T_{pw}) proposed by Inoue [29] was one of the most frequently used parameters determining the glass stability [30]. However, this parameter may not take into account enough thermal factors for analysis of fibre drawing from melts, which mostly relates to the glass behaviour around T_m and T_l . Therefore, another parameter proposed by Hruby [31],

$$K_{gl} = \frac{T_{c,ons} - T_g}{T_l - T_{c,ons}}$$

was employed for the thermal stability analysis. In addition, K_{gt} has already been used by Arstila et al. [32] to compare different bioactive glass compositions suitable for fibre drawing directly from melts. Similar to T_{pw} , higher values of K_{gt} denote higher thermal stability of the glass against crystallisation upon reheating [30, 31].

2.6. Thermomechanical analysis

Thermal expansion coefficient (α) was measured using a thermomechanical analyser (TA Instruments TMA Q400, UK). During measuring, a sample in 7 mm height and 9 mm diameter was heated at a rate of 5 °C min⁻¹ with an applied load of 50 mN. The value of α was taken as an average between 50 °C and 250 °C, and automatically calculated using the equation:

$$\alpha = \frac{\Delta L}{L} \cdot \frac{1}{\Delta T}$$

where ΔL is the increase in the original length L of the rod and ΔT is the temperature interval over which the sample is heated [33].

2.7. Density analysis

The density of the samples was measured using an Archimedes method. After weighing in dry as m_{dry} , the bulk glass was immersed in the ethanol (C₂H₆O, Sigma Aldrich, UK; $\rho_{ethanol} = 0.789$ kg L⁻¹ at 25 °C) and weighed as m_{wet} . Then the density of the bulk glass (ρ_{glass}) was obtained as follows:

$$\rho_{glass} = \frac{m_{dry}}{m_{dry} - m_{wet}} \cdot \rho_{ethanol}$$

2.8. Degradation analysis

Glass rods of Ø10 mm were cut into 10 mm height using a low-speed saw (South Bay Technologies; California, USA) equipped with a diamond blade (Buehler; Coventry, UK) and lubricated with ethanol (Fisher Chemicals, UK). The cut rod was put into a glass vial containing 30 mL phosphate buffer saline solution (PBS; pH = 7.4 ± 0.1) and placed into an oven at 37.0 ± 0.5 °C. At specified time points, the vial was removed and the solution pH was measured. Meanwhile, the dimensions and mass of the glass rod were measured after blotting dry with tissue. The whole analysis was carried out for 41 days (time points of 0, 1, 2, 3, 7, 9, 13, 16, 20, 23, 27, 30, 34, 37 and 41) and the PBS solution was changed at each time point. The mass loss percentage (%) and mass loss per unit area (kg m⁻²) at each time point were calculated using:

$$\text{mass loss (\%)} = \frac{m_o - m_t}{m_o}$$

$$\text{mass loss per unit area} = \frac{m_o - m_t}{A_t}$$

where m_o is the initial mass of the glass rod measured on day 0; m_t and A_t is the mass and surface area respectively at time point t. Graphs plotted were weight loss per unit area against time and the slope of the graphs gave the degradation rate in terms of $\text{kg m}^{-2} \text{s}^{-1}$.

2.9. Statistical analysis

Measured data were analysed using a student's unpaired t-test, assuming equal variance. The two-tailed p -value was determined and defined as $p > 0.05$ (statistically insignificant), $p < 0.05$ (statistically significant), $p < 0.01$ (very statistically significant) and $p < 0.0001$ (extremely statistically significant).

3. Results

3.1. ICP analysis

The composition of the samples confirmed by ICP-MS is shown in Table 2. The differences in P_2O_5 , B_2O_3 , CaO, MgO and Fe_2O_3 contents observed in this study are of ± 1.6 , ± 0.3 , ± 1.3 , ± 0.8 and ± 0.4 mol%.

Table 2 Glass compositions confirmed by ICP-MS, in mol% ($n = 3$).

Sample codes		P_2O_5	B_2O_3	Na_2O	CaO	MgO	Fe_2O_3	O/P
Ca(29-x)Mg16Fe(x)	Ca24Mg16Fe5	44.0 ± 0.1	4.8 ± 0.1	6.2 ± 0.1	23.0 ± 0.1	16.8 ± 0.1	5.3 ± 0.1	3.37
	Ca21Mg16Fe8	43.6 ± 0.1	4.8 ± 0.1	6.7 ± 0.1	20.3 ± 0.1	16.2 ± 0.1	8.4 ± 0.1	3.45
	Ca18Mg16Fe11	43.4 ± 0.1	4.7 ± 0.1	7.3 ± 0.1	17.4 ± 0.1	16.0 ± 0.1	11.2 ± 0.1	3.52
Ca24Mg(21-x)Fe(x)	Ca24Mg16Fe5	44.0 ± 0.1	4.8 ± 0.1	6.2 ± 0.1	23.0 ± 0.1	16.8 ± 0.1	5.3 ± 0.1	3.37
	Ca24Mg13Fe8	43.8 ± 0.1	4.9 ± 0.1	6.8 ± 0.1	23.1 ± 0.1	13.2 ± 0.1	8.2 ± 0.1	3.44
	Ca24Mg10Fe11	43.7 ± 0.1	4.8 ± 0.1	7.3 ± 0.1	22.7 ± 0.1	10.1 ± 0.1	11.3 ± 0.1	3.51

3.2. XRD analysis

The absence of any sharp crystalline peaks on the XRD traces in Fig 1 specified the amorphous nature of the samples.

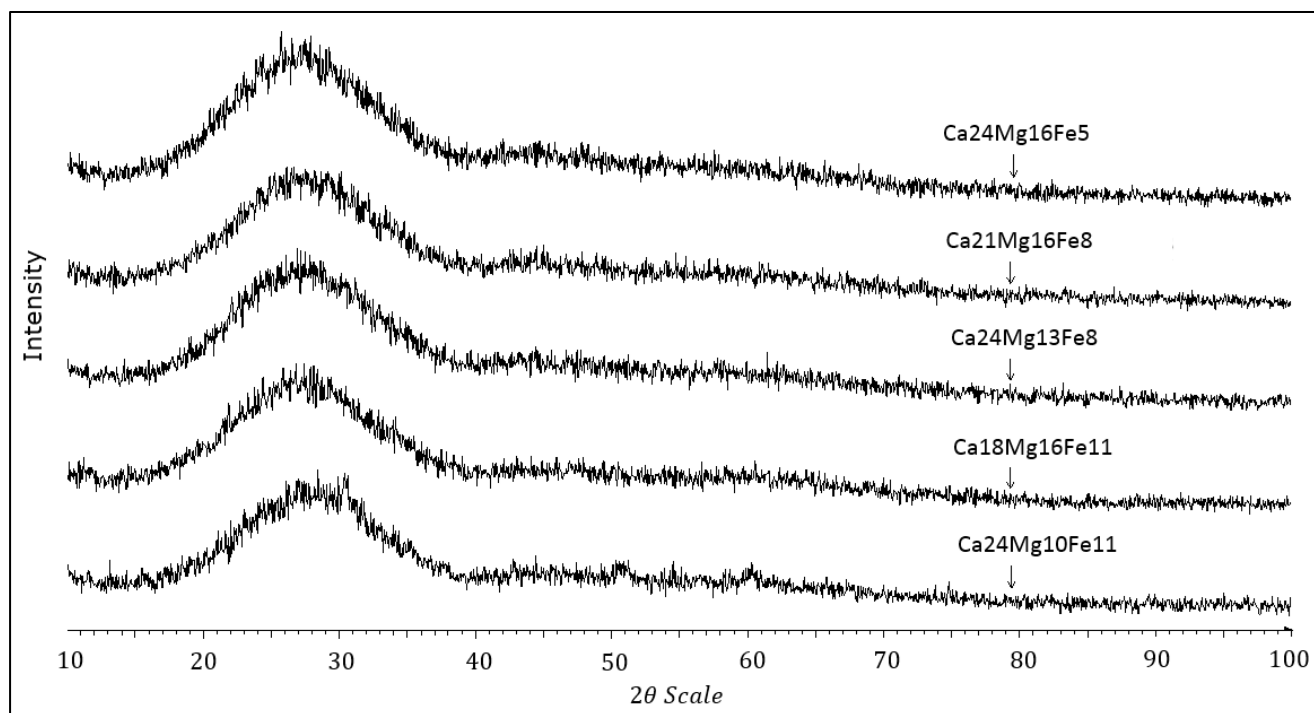


Fig 1 XRD data confirmed the amorphous structure of the samples.

3.3. FTIR analysis

FT-IR analysis was carried out to verify the structural changes of the glasses. The five bands observed in Fig 2 were at ~ 530 , ~ 760 , ~ 920 , ~ 1100 and ~ 1260 cm^{-1} , with high similarity to those reported for other PBGs [34-36] and their peak assignments are provided in Table 3.

As shown in Fig 2(a), the band at 527 cm^{-1} shifted to a higher wavenumber and the intensity of the band at 761 cm^{-1} decreased for a higher Fe_2O_3 content at the cost of CaO . A similar variation was observed for the band at 919 cm^{-1} . Meantime, the band at 1095 cm^{-1} was seen to be broader with reduced intensity and the band at ~ 1260 cm^{-1} was noticed to shift to lower wavenumbers and be broader with reduced intensity. Similar trends were observed from Fig 2(b) for the glasses with increasing Fe_2O_3 content at the cost of MgO .

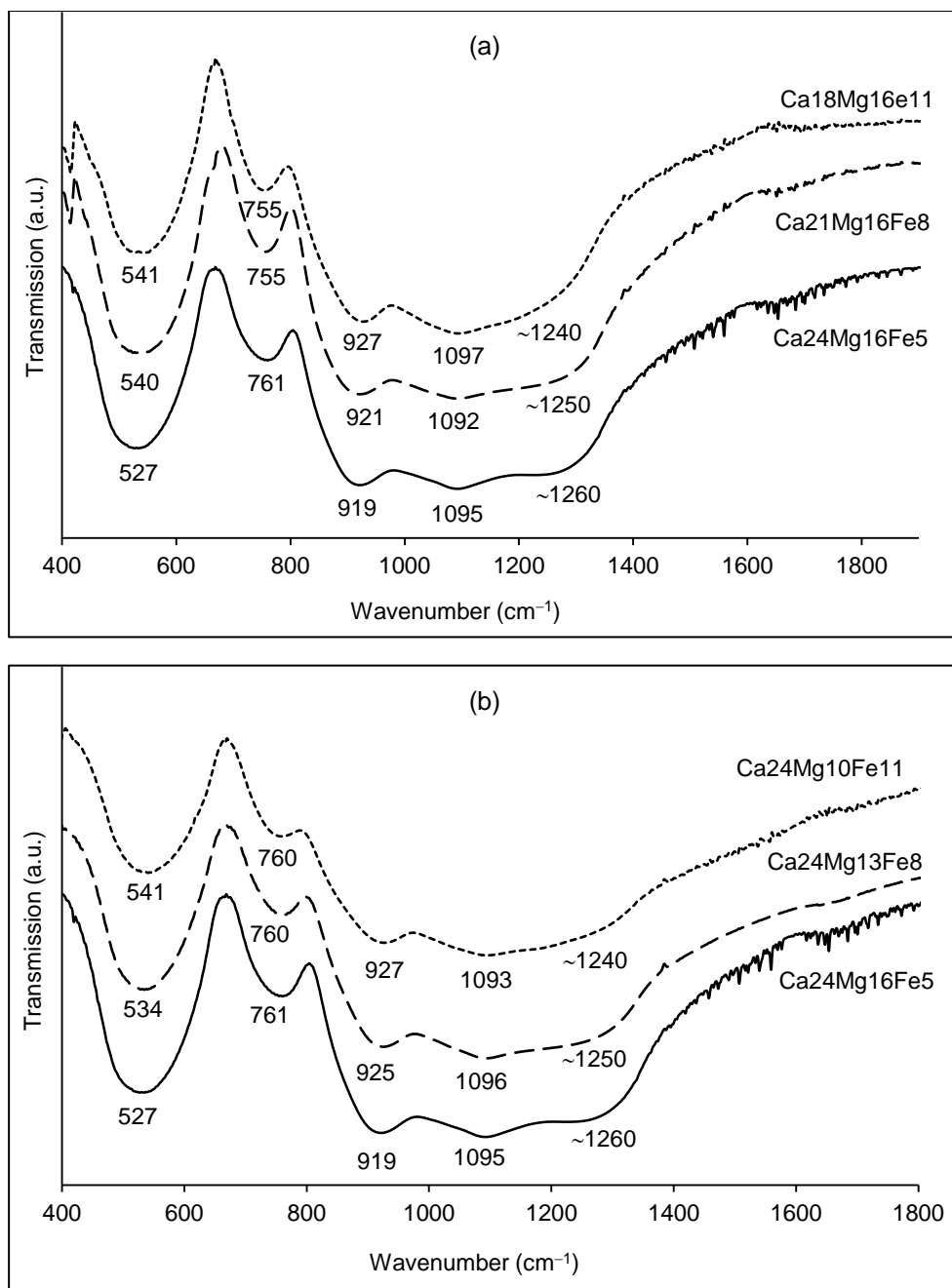


Fig 2 FTIR spectrum for the samples against Fe₂O₃ content at the cost of CaO (a) and MgO (b).

Table 3 FTIR band assignments.

Wavenumbers (cm ⁻¹)	Assignments	Ref.
527-541	$\delta_{as}(\text{O-P-O})$, asymmetric bending mode of O-P-O in Q ¹ species	[37-40]
755-761	$\nu_s(\text{P-O-P})$, symmetric stretching mode of the bridging oxygen bonded to a phosphorous atom in Q ² species	[38, 39, 41]

919-927	$\nu_{as}(\text{P-O-P})$, asymmetric stretching mode of the bridging oxygen bonded to a phosphorous atom in Q^2 species	[41, 42]
1092-1097	$\nu_s(\text{PO}_3)^{2-}$ and $\nu_{as}(\text{PO}_3)^{2-}$, symmetric and asymmetric stretching modes of the chain terminating Q^1 groups	[38, 41, 42]
1240-1260	$\nu_{as}(\text{PO}_2)^-$, symmetric stretching mode of the two non-bridging oxygens bonded to a phosphorous atom in Q^2 species	[37, 40, 41]

3.4. Thermal analysis

Fig 3 displays the thermal traces obtained from DSC analysis. Fig 4 showed a linear increase in T_g against Fe_2O_3 content, whilst the replacement of MgO was seen to have an insignificant ($p > 0.05$) effect on T_g with the replacement of CaO. Moreover, two crystallisation peaks (T_c) were observed for all the glasses investigated, however, three melting peaks (T_m) were found for the 11 mol% Fe_2O_3 compositions, which may have been due to overlapping of some crystallisation peaks.

Table 4 gives a summary of $T_{c,ons}$, T_c , T_m , T_l , T_{pw} and K_{gl} values of the samples. It was observed that T_l increased with increasing Fe_2O_3 content for all the glasses. $T_{c,ons}$ increased by ~ 1.2 °C with an increment of 3 mol% Fe_2O_3 at the expense of CaO, while it showed a non-linear variation when MgO was replaced by Fe_2O_3 .

As seen in Fig 5(a), T_{pw} decreased by 2.7 °C with an increase of 3 mol% in Fe_2O_3 content each time at the cost of CaO, whilst it decreased by 5.2 °C as Fe_2O_3 content increased from 5 to 8 mol% at the cost of MgO and increased again by 6.6 °C in the 11 mol% Fe_2O_3 composition. Quite similar trends were exhibited in Fig 5(b) for K_{gl} .

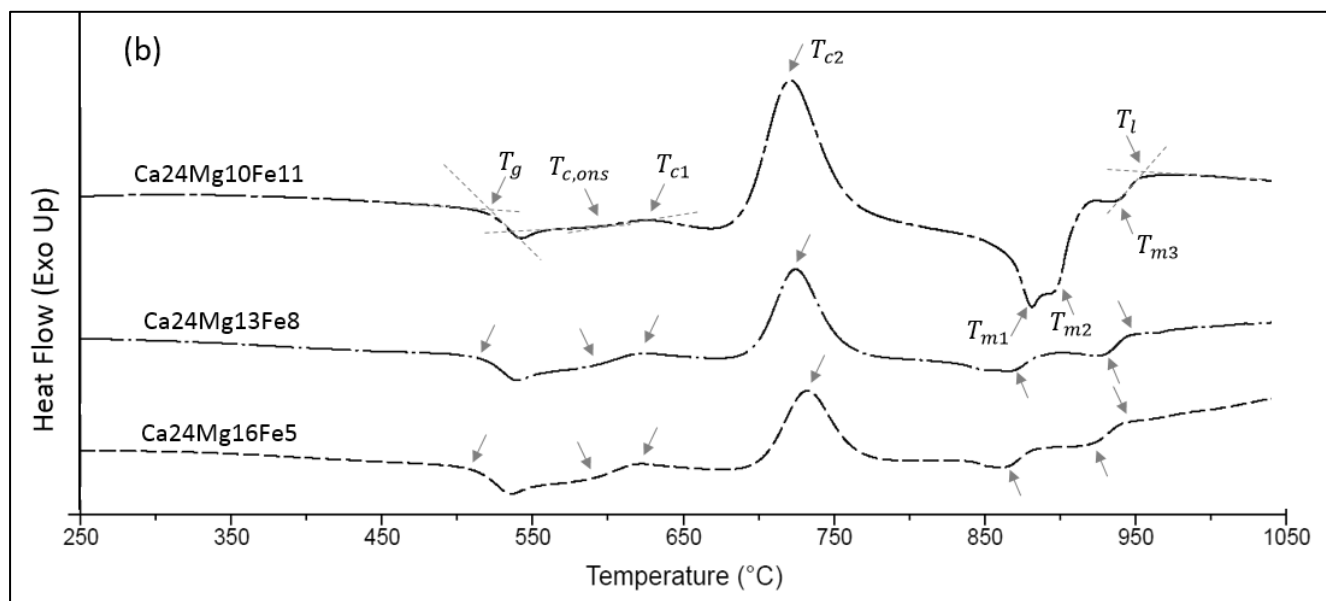
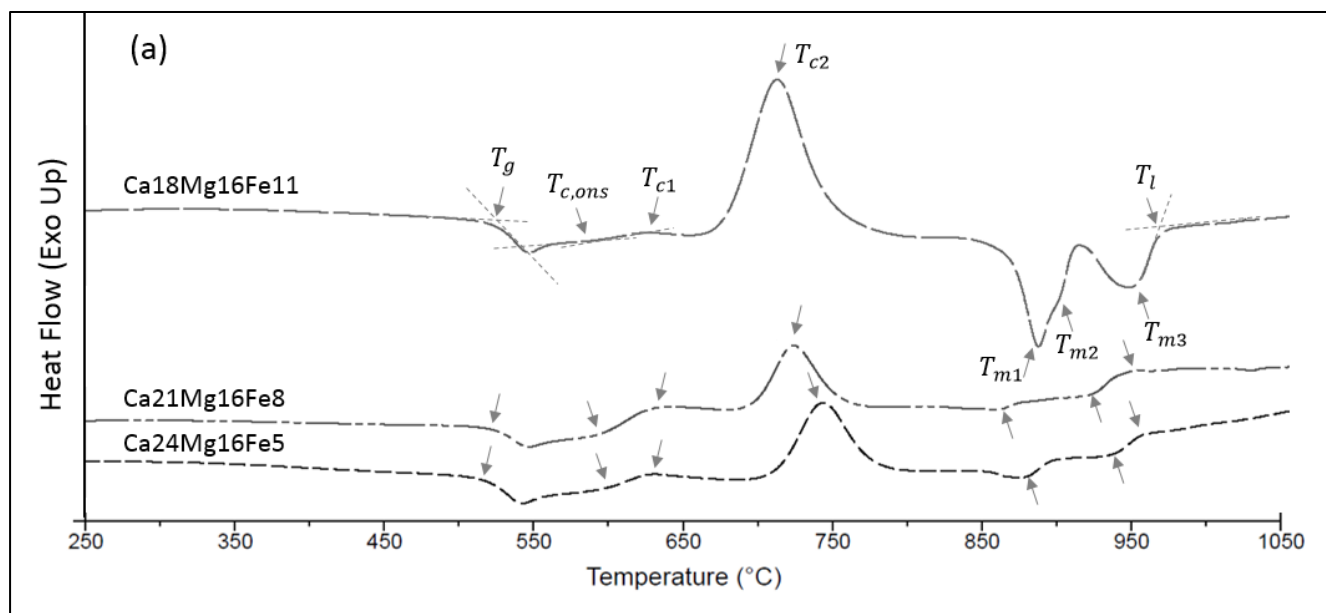


Fig 3 Thermal scans for the samples against Fe₂O₃ content at the cost of CaO (a) and MgO (b).

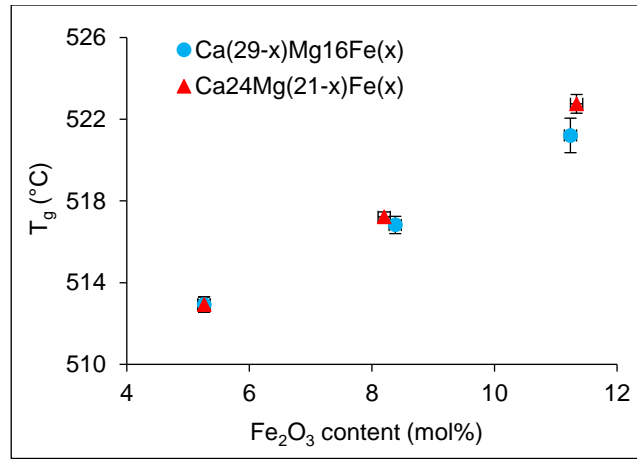


Fig 4 Glass transition temperature (T_g) presents a linear increase against Fe_2O_3 content for the samples ($n = 3$).

Table 4 Thermal characteristics ($T_{c,ons}$, T_c , T_m and T_l) for the samples ($n = 3$).

Sample codes		$T_{c,ons}$ (°C)	T_c (°C)	T_m (°C)	T_l (°C)	T_{pw} (°C)	K_{gl}
Ca(29-x)Mg16Fe(x)	Ca24Mg16Fe5	586.0 ± 1.8	619.8 ± 2.6	839.7 ± 3.3	918.2 ± 1.3	73.1 ± 3.3	0.220 ± 0.011
			722.1 ± 0.3	898.0 ± 1.6			
	Ca21Mg16Fe8	587.2 ± 1.5	619.9 ± 0.3	823.7 ± 1.3	925.8 ± 1.0	70.4 ± 2.5	0.208 ± 0.008
			712.7 ± 0.2	904.4 ± 2.0			
	Ca18Mg16Fe11	588.4 ± 1.2	618.7 ± 0.1	854.5 ± 1.3	932.7 ± 2.9	67.7 ± 0.7	0.197 ± 0.005
				868.3 ± 0.2			
913.2 ± 1.1							
Ca24Mg(21-x)Fe(x)	Ca24Mg16Fe5	586.0 ± 1.8	619.8 ± 2.6	839.7 ± 3.3	918.2 ± 1.3	73.1 ± 3.3	0.220 ± 0.011
			722.1 ± 0.3	898.0 ± 1.6			
	Ca24Mg13Fe8	585.1 ± 0.2	616.4 ± 5.5	832.1 ± 0.0	921.1 ± 0.8	67.9 ± 0.1	0.202 ± 0.001
				715.6 ± 0.2			
	Ca24Mg10Fe11	597.2 ± 0.2	628.5 ± 2.0	862.9 ± 0.4	930.9 ± 0.3	74.4 ± 0.6	0.223 ± 0.002
				875.8 ± 1.2			
			712.3 ± 0.1	917.3 ± 0.3			

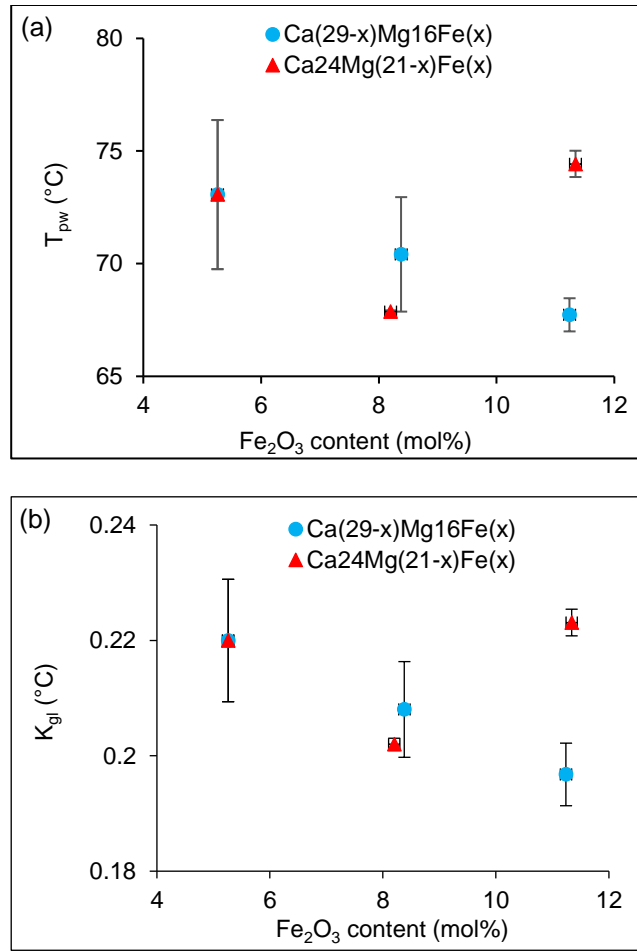


Fig 5 Parameters of glass stability: (a) the processing window, $T_{pw} = T_{c,ons} - T_g$ and (b) $K_{gl} = (T_{c,ons} - T_g)/(T_l - T_{c,ons})$ of the samples ($n = 3$).

3.5. Thermomechanical analysis

As shown in Fig 6, the thermal expansion coefficient (α) decreased by $10.82 > 10.57 > 10.35 \times 10^{-6} \text{ °C}^{-1}$ against Fe₂O₃ content at the cost of CaO, while a non-linear variation ($10.82, 10.63$ and $10.75 \times 10^{-6} \text{ °C}^{-1}$) was observed when MgO was replaced by increasing Fe₂O₃.

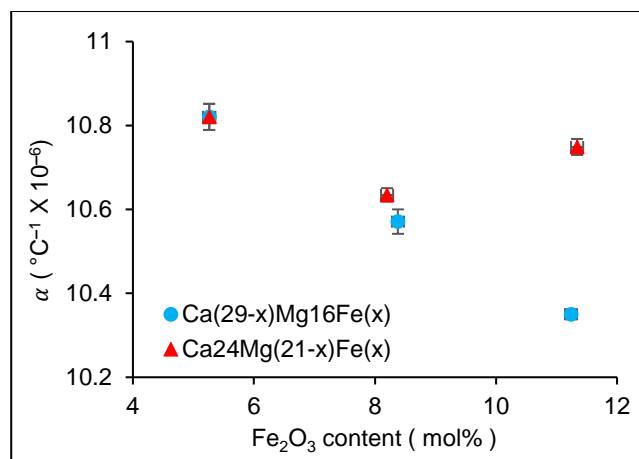


Fig 6 Thermal expansion coefficient (α) of the samples ($n = 3$).

3.6. Density analysis

Fig 7 shows a linear increase in density (ρ) as the Fe_2O_3 content increased in the glasses. The ρ -values were 2.76, 2.83 and $2.87 \times 10^6 \text{ kg m}^{-3}$ for 5, 8 and 11 mol% Fe_2O_3 compositions respectively expending CaO, and were 2.76, 2.83 and $2.89 \times 10^6 \text{ kg m}^{-3}$ with increasing Fe_2O_3 at the expense of MgO.

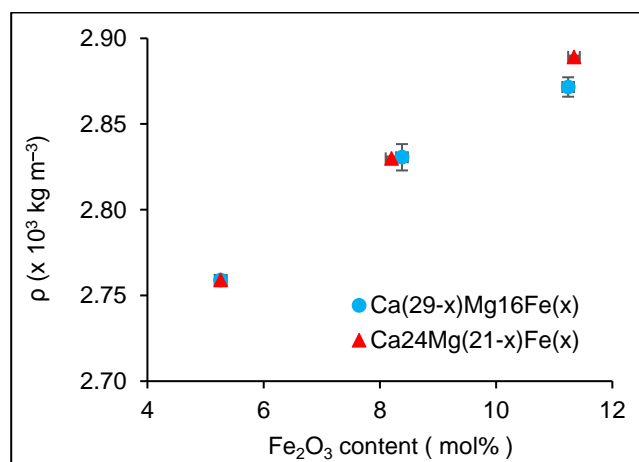


Fig 7 Density (ρ) shows a linear increase against Fe_2O_3 content for the samples ($n = 3$).

3.7. Degradation analysis

Fig 8 shows the mass loss (%) of glass rods as a function of immersion time in PBS solution at 37°C and Fig 9 represents the corresponding degradation rate in $\text{kg m}^{-2} \text{ s}^{-1}$. As expected, a linear decrease in degradation rate ($12.08 > 9.03 > 5.02 \times 10^{-5} \text{ kg m}^{-2} \text{ s}^{-1}$) was observed for the glasses with increasing Fe_2O_3 content with decreasing CaO content.

Similarly, the degradation rate decreased by $12.08 > 8.67 > 4.62 \times 10^{-5} \text{ kg m}^{-2} \text{ s}^{-1}$ when MgO was replaced by Fe_2O_3 . In contrast, the replacement of MgO had an insignificant ($p > 0.05$) effect on the decrease of degradation rate as compared with the replacement of CaO. In addition, the pH values for all the glasses containing different Fe_2O_3 contents were observed to maintain a consistent value of $\text{pH } 7.40 \pm 0.02$ for the entire duration of the degradation study (41 days).

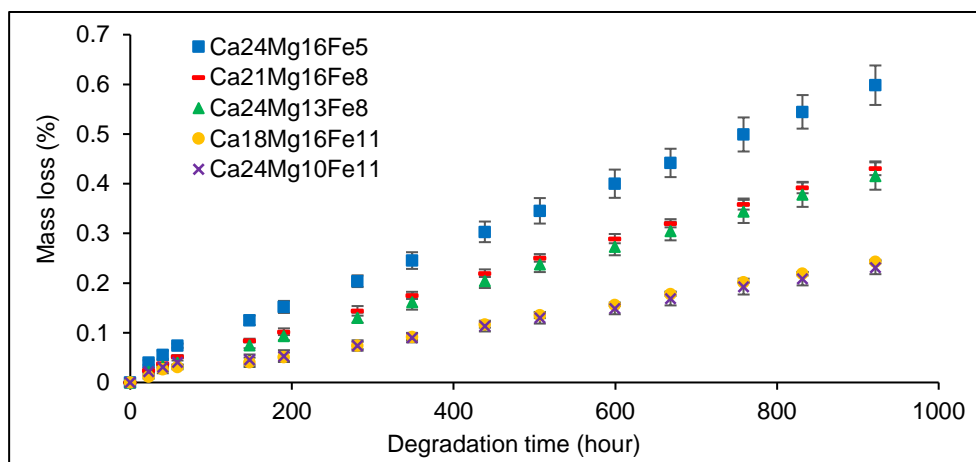


Fig 8 Mass loss (%) of the glass rods investigated in PBS solution at 37°C for 41 days ($n = 3$).

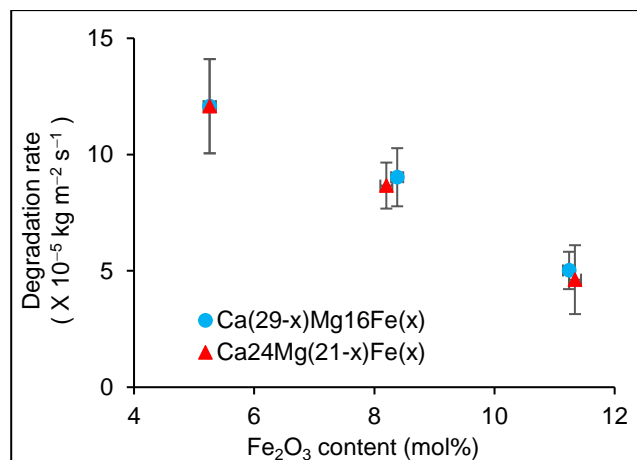


Fig 9 Degradation rate of the glass rods shows a linear increase against Fe_2O_3 content ($n = 3$).

4. Discussion

4.1. FTIR analysis

It is well known that the structure of PBGs is strongly dependent on the O/P ratio in the glass compositions, which is modified by the addition of different metal oxides [43, 44]. The pure phosphate network consists of a series of PO_4 tetrahedra connecting to adjacent units by three bridging oxygens. The network connectivity can be described in terms of Q^n terminology, where n is the number of bridging oxygens per phosphate unit. Q^3 corresponds to ultraphosphates (O/P = 2.5), Q^2 to metaphosphates (O/P = 3), Q^1 to pyrophosphates (O/P = 3.5) and Q^0 to orthophosphates (O/P = 4). In this study, all the samples were shown to be amorphous (see Fig 1) and were compositionally confirmed by ICP-MS (see Table 2). Following, the FTIR band assignment in Table 3 showed that the local phosphate network was mainly based on pyro- and metaphosphate units (Q^1 and Q^2), even though the O/P ratio was higher than 3.5 (see Table 2). This was suggested to be due to the introduction of BO_3 and BO_4 units into the phosphate chain structure [45], forming a mixed borophosphate glass.

As shown in Fig 2(a), the absorption band at 527 cm^{-1} shifted to higher wavenumbers for higher Fe_2O_3 content compositions at the cost of CaO. Bergo et al. [34] found a band at $\sim 500\text{ cm}^{-1}$ for the 3.2 mol% Fe_2O_3 composition in the $\text{P}_2\text{O}_5\text{-Fe}_2\text{O}_3\text{-BaO}$ system and Lu et al. [37] observed one at 549 cm^{-1} in the $\text{P}_2\text{O}_5\text{-Fe}_2\text{O}_3\text{-TiO}_2\text{-CaF}_2$ glass with 40 mol% Fe_2O_3 . Both of them attributed their band to the overlapping vibrations of Fe-O-P bonds and O-P-O in Q^1 units. Magdas et al. [39] also assigned a band at 584 cm^{-1} to Fe-O-P bonds in the $\text{P}_2\text{O}_5\text{-Fe}_2\text{O}_3\text{-PbO}$ system. Therefore, the band-shift from 527 cm^{-1} was suggested to be due to the increase in Fe-O-P bonds, as a result of the increase in Fe_2O_3 content.

The intensity of the bands at 761 and 919 cm^{-1} was seen to reduce with increasing Fe_2O_3 at the cost of CaO; that is, the symmetric and asymmetric vibrations of the bridging oxygen in the P-O-P linkage of the Q^2 unit became weaker. Given that the glasses with a higher amount of Fe_2O_3 have a higher O/P ratio, the reduction of the intensity indicated a quantitative loss of Q^2 species and a higher degree of depolymerisation of the phosphate chains [41, 46]. Muresan et al. [36] also found such a depolymerisation process of the phosphate network in the $\text{P}_2\text{O}_5\text{-Fe}_2\text{O}_3\text{-CaO-Na}_2\text{O}$ glass and attributed it to the addition of iron oxides.

The broad band around 1100 cm^{-1} was assigned to the overlap of symmetric and asymmetric vibrations of the P-O^- groups in Q^1 units [38, 42]. Sharmin et al. [41] tracked such an overlap with B_2O_3 additions. Further, this band at 1095 cm^{-1} was seen to be broader with reduced intensity as the amount of Fe_2O_3 increased, which was suggested to be due to the formation of Fe-O-P linkages [47].

A significant change was realised at $\sim 1260\text{ cm}^{-1}$ as this peak became broader and weaker. This decrease in the non-bridging $(\text{PO}_2)^-$ groups intimated a progressive increase in the connectivity of the glass with Fe_2O_3 , again due to the formation of Fe-O-P linkages instead of P-O-P bonds [47].

Among the instances given above for the discussion of Q species, Carta et al. [46] and Sharmin et al. [41] conducted ^{31}P solid state MAS NMR spectroscopy to evidence the inference from FTIR data of phosphate and borophosphate glasses, respectively. Moreover, Kim et al. [47] and Muresan et al. [36] employed Raman spectroscopy to confirm the FTIR results of iron-containing phosphate glasses, while Bergo et al. [34] used Mössbauer spectroscopy to investigate $\text{Fe}^{2+}/\text{Fe}^{3+}$ ratio. Therefore, the FTIR data was considered as a qualitative indicator of the Q species present and as a comparator analysis in this study. In this study attempts were made to perform structural analysis of the glass using ^{31}P and ^{11}B solid state NMR. However, the magnetic character of the iron led to line broadening and resulted in an intense manifold of spinning sidebands. As a result it was not possible to resolve the structural data and thus the NMR was not included in this paper.

4.2. Thermal analysis

It is well established that CaO, MgO and Fe_2O_3 addition can increase the T_g of PBGs when they individually replace Na_2O or P_2O_5 in the glass system [15, 17]. In this study, DSC results showed a linear increase in T_g against Fe_2O_3 content for all the glasses investigated (see Fig 4), even though the CaO or MgO content decreased simultaneously. Elisa et al. [11, 48] found that the substitution of MgO by CaO caused an increase in T_g by $27\text{ }^\circ\text{C}$ in the samples without iron, but almost no modification on T_g in the iron-containing samples. It was also noticed that the value of T_g increased by $\sim 5\text{ }^\circ\text{C}$ with an increment of 3 mol% in Fe_2O_3 content at the cost of CaO/MgO (see Fig 4). By contrast, Sharmin et al. [7] recorded an increase of $\sim 15\text{ }^\circ\text{C}$ in T_g when Fe_2O_3 increased from 3 to 5 mol% replacing Na_2O in the $45\text{P}_2\text{O}_5\text{-}5\text{B}_2\text{O}_3\text{-}16\text{CaO}\text{-}24\text{MgO}\text{-}(x)\text{Fe}_2\text{O}_3\text{-}(10\text{-}x)\text{Na}_2\text{O}$ system. In general, the increase of T_g was associated with a denser cross-linking between the phosphate chains caused by the higher Me-O bond strength [17, 49], with the ionic

radius decreasing for $\text{Na}^+(1.13 \text{ \AA}) > \text{Ca}^{2+}(0.99 \text{ \AA}) > \text{Mg}^{2+}(0.72 \text{ \AA}) > \text{Fe}^{3+}(0.64 \text{ \AA})$ (six-fold coordination for Mg^{2+} and Ca^{2+}) [26, 50].

The shifts of T_{c2} peaks shown in Fig 3(a) and (b) evidenced a promotion in crystal growth with Fe_2O_3 addition and the smaller shift in (b) compared to the one in (a) also suggested a greater promotion of crystal growth by MgO than CaO. The increase in numbers of T_m peaks by increasing Fe_2O_3 to 11 mol% was an indication of the presence of more crystalline phases within the composition. A similar increase was also found by Ahmed et al. [15].

The glass stability was determined using two parameters: T_{pw} and K_{gl} . Hruby [31] reported that the interval $T_{c,ons} - T_g$ was directly proportional to the glass-forming tendency and Arstila et al. [32] stated that the higher K_{gl} of a glass indicated higher suitability for fibre drawing directly from melts. As seen in Fig 5(a), the T_{pw} shows a linear decrease as Fe_2O_3 replaced CaO. However, the value of T_{pw} decreased by 7.1% as Fe_2O_3 increased from 5 to 8 mol% at the cost of MgO, and then increased by 9.6% when Fe_2O_3 increased to 11 mol%. Similar trends were observed on K_{gl} in Fig 5(b). By using $T_c - T_g$ to indicate the stability of binary phosphate glasses, Sahar et al. [22] obtained a linear decrease of stability with decreasing CaO and an anomalous variance with decreasing MgO. They also found a structural change from MgP_2O_6 to $\text{Mg}_2\text{P}_2\text{O}_7$ in different MgO- P_2O_5 compositions, while only one phase, $\text{Ca}_3(\text{PO}_4)_2$, occurred in all the compositions of the CaO- P_2O_5 glasses. Furthermore, basing on the data in Fig 4 and Table 4, the $T_{c,ons}$ -value seemed to dominate the variance of T_{pw} ; that is, the variance of stability could be considered more basing on the crystallisation behaviour of the investigated glasses rather than T_g . Stefan and Karabulut [14] also found that the crystallisation tendency increased with Fe_2O_3 and the crystal observed were $\text{Fe}_2\text{P}_4\text{O}_{12}$, BPO_4 , $\text{Ca}_2\text{P}_2\text{O}_7$, $\text{Ca}_3(\text{PO}_4)_2$, $\text{Mg}_2\text{P}_2\text{O}_7$ and $\text{B}_{0.57}\text{Fe}_{0.43}\text{PO}_4$ phases, especially for $x \geq 10$ mol% compositions in the $(55-x)\text{P}_2\text{O}_5-(x)\text{Fe}_2\text{O}_3-10\text{B}_2\text{O}_3-30\text{CaO}-5\text{MgO}$ glasses. Massera et al. [51] reported that the formation of Fe-O-P bonds would also increase the glass crystallisation tendency by decreasing the numbers of non-bridging oxygens.

4.3. Thermomechanical analysis

According to Shih et al. [52], the thermal expansion coefficient (α) is sensitive to the cross-link density and the interaction of cations with non-bridging oxygens in the PBGs. As shown in Fig 6, the α -value decreased against mol% of Fe_2O_3 at the cost of CaO, which was suggested to be due to the increase of the cationic field strength in the glass network [48]. The cationic field strength was given by Z/r^2 , where Z is the cation charge and r is the cationic radius [53].

It was also seen in Fig 6 that the α decreased as Fe_2O_3 increased from 5 to 8 mol% at the expense of MgO and rose up again with Fe_2O_3 of 11 mol%. This anomalous behaviour was suggested to be associated with the abrupt change of the coordination equilibrium of Mg^{2+} in the glass network [54]. McMillan [55] explained an increase of α in the silicate glass structure by using the lower electrostatic bond strengths of the cations, which was defined as $Z/N_{\text{Me-O}}$, where $N_{\text{Me-O}}$ is the coordination number of the metal cation. Hoppe et al. [23] have investigated the binary P_2O_5 -MgO glass and found a reduction in $N_{\text{Mg-O}}$ from 6 to 4 with an increased O/P ratio in the ultra- to metaphosphate composition range. In this study, the more complex borophosphate glass system may have caused similar behaviour but in a different compositional range, which lowered the $N_{\text{Mg-O}}$ and resulted in a higher α -value for the 11 mol% Fe_2O_3 composition.

4.4. Density analysis

The ρ -value shown in Fig 7 indicated an increase with Fe_2O_3 content, which is in good agreement with other published works [20, 26, 56]. This increase was associated with the higher field strength of iron ions compared to calcium and magnesium, which led to stronger cross-linking and a more dense glass [53]. Hasan et al. [57] reported an increase in density with increasing iron content in the P_2O_5 - Fe_2O_3 - Na_2O -CaO-MgO glass. They recommended that the density of the bulk glass was an important tool to measure the cross-link density and the packing structure of atoms, and the increased density with increasing Fe_2O_3 content was due to the formation of Fe-O-P bonds. Similar results were also presented by Yu et al. [13].

4.5. Degradation analysis

Yu et al. [13] have investigated the dissolution property of the P_2O_5 - Fe_2O_3 - Na_2O glass and suggested that the increased durability of PBGs with increasing Fe_2O_3 was attributed to the replacement of P-O-P bonds by more chemically resistant P-O-Fe(II) and P-O-Fe(III) bonds. Ahmed et al. [15] and Hasan et al. [57] also reported that Fe_2O_3 addition improved the chemical durability of the P_2O_5 - Fe_2O_3 - Na_2O -CaO and P_2O_5 - Fe_2O_3 - Na_2O -CaO-MgO glasses, respectively. They suggested that the improvement was due to the replacement of P-O-P bonds with more hydration resistant Fe-O-P bonds and the increased cross-linking between the phosphate chains. In all the investigations above, the substitution was performed between Fe_2O_3 and Na_2O , while in this study, the Fe_2O_3 was added to replace CaO and MgO. It is well known that CaO, MgO and Fe_2O_3 can all improve the durability of PBGs [17, 57], whilst the results

in Fig 8 and Fig 9 showed that Fe₂O₃ was much more effective in decreasing the degradation rates of PBGs as compared to CaO/MgO.

In summary, the above studies showed a linear increase in glass transition temperature (T_g), density (ρ) and chemical durability with increasing Fe₂O₃ content at the expense of CaO/MgO, which was suggested to be due to further depolymerisation and stronger cross-linking of the phosphate chains. Moreover, the replacement of CaO by Fe₂O₃ content linearly decreased the glass stability (T_{wp} and K_{gl}) and thermal expansion coefficient (α) of the PBGs. However, the replacement of MgO led to a decrease in T_{wp} , K_{gl} and α as Fe₂O₃ content increased from 5 to 8 mol%, and then increased again when Fe₂O₃ content increased from 8 to 11 mol%. Furthermore, future work will investigate manufacturing fibres from the above formulations produced.

5. Conclusions

Structural analysis suggested depolymerisation and stronger cross-linking for the phosphate chains as the Fe₂O₃ content increased at the cost of CaO/MgO, resulting in an increase of T_g , ρ and chemical durability of the glasses. The B₂O₃ addition increased the phosphate chain length, which could benefit the fibre drawing process. The glass stability parameters indicated that higher CaO/MgO ratios would also have a positive effect on the fibre drawing performance of glasses with high Fe₂O₃ content. Future work will investigate drawing fibres from the formulations produced and characterising the mechanical properties of the glass fibres formed.

6. Reference

- [1] A. J. Parsons, I. Ahmed, P. Haque, B. Fitzpatrick, M. I. K. Niazi, G. S. Walker, *et al.*, "Phosphate Glass Fibre Composites for Bone Repair," *J Bionic Eng*, vol. 6, pp. 318-323, 2009.
- [2] I. Ahmed, M. Lewis, I. Olsen, and J. C. Knowles, "Phosphate glasses for tissue engineering: Part 1. Processing and characterisation of a ternary-based P₂O₅-CaO-Na₂O glass system," *Biomaterials*, vol. 25, pp. 491-499, 2004.
- [3] I. Ahmed, I. A. Jones, A. J. Parsons, J. Bernard, J. Farmer, C. A. Scotchford, *et al.*, "Composites for bone repair: phosphate glass fibre reinforced PLA with varying fibre architecture," *J Mater Sci-Mater M*, vol. 22, pp. 1825-1834, 2011.
- [4] N. Sharmin, A. J. Parsons, C. D. Rudd, and I. Ahmed, "Effect of boron oxide addition on fibre drawing, mechanical properties and dissolution behaviour of phosphate-based glass fibres with fixed 40, 45 and 50 mol% P₂O₅," *J Biomater Appl*, vol. 29, pp. 639-53, Nov 2014.
- [5] D. S. Brauer, "Phosphate Glasses," in *Bio-Glasses: An Introduction*, J. R. Jones and A. G. Clare, Eds., ed UK: John Wiley and Sons, Ltd., 2012, pp. 45-64.
- [6] I. Ahmed, M. Lewis, I. Olsen, and J. C. Knowles, "Phosphate glasses for tissue engineering: Part 2. Processing and characterisation of a ternary-based P₂O₅-CaO-Na₂O glass fibre system," *Biomaterials*, vol. 25, pp. 501-507, 2004.

- [7] N. Sharmin, C. D. Rudd, A. J. Parsons, and I. Ahmed, "Structure, viscosity and fibre drawing properties of phosphate-based glasses: effect of boron and iron oxide addition," *J Mater Sci*, vol. 51, pp. 7523-7535, 2016.
- [8] M. A. Ouis, A. M. Abdelghany, and H. A. ElBatal, "Corrosion mechanism and bioactivity of borate glasses analogue to Hench's bioglass," *Processing and Application of Ceramics*, vol. 6, pp. 141–149, 2012.
- [9] H. Fu, Q. Fu, N. Zhou, W. Huang, M. N. Rahaman, D. Wang, *et al.*, "In vitro evaluation of borate-based bioactive glass scaffolds prepared by a polymer foam replication method," *Materials Science and Engineering C*, vol. 29, pp. 2275-2281, 2009.
- [10] C. Albon, D. Muresan, R. E. Vandenberghe, and S. Simon, "Iron environment in calcium-soda-phosphate glasses and vitroceraamics," *J Non Cryst Solids*, vol. 354, pp. 4603-4608, 2008.
- [11] M. Elisa, R. Iordanescu, B. A. Sava, G. Aldica, V. Kuncser, C. Valsangiacom, *et al.*, "Optical and structural investigations on iron-containing phosphate glasses," *J Mater Sci* vol. 46, pp. 1563-1570, 2010.
- [12] B. C. Sales and L. A. Boatner, "Physical and chemical characteristics of lead-iron phosphate nuclear waste glasses," *J Non Cryst Solids*, vol. 79, pp. 83-116, 1986.
- [13] X. Yu, D. E. Day, G. J. Long, and R. K. Brow, "Properties and structure of sodium-iron phosphate glasses," *J Non Cryst Solids*, vol. 215, pp. 21-31, 1997.
- [14] R. Stefan and M. Karabulut, "Structural properties of iron containing calcium-magnesium borophosphate glasses," *J Mol Struct*, vol. 1071, pp. 45-51, 2014.
- [15] I. Ahmed, C. A. Collins, M. P. Lewis, I. Olsen, and J. C. Knowles, "Processing, characterisation and biocompatibility of iron-phosphate glass fibres for tissue engineering," *Biomaterials*, vol. 25, pp. 3223-32, Jul 2004.
- [16] P. A. Bingham, R. J. Hand, S. D. Forder, and A. Lavaysierre, "Vitrified metal finishing wastes II. Thermal and structural characterisation," *J Hazard Mater*, vol. 122, pp. 129-38, Jun 30 2005.
- [17] I. Ahmed, A. Parsons, A. Jones, G. Walker, C. Scotchford, and C. Rudd, "Cytocompatibility and effect of increasing MgO content in a range of quaternary invert phosphate-based glasses," *J Biomater Appl*, vol. 24, pp. 555-75, Feb 2010.
- [18] K. Franks, V. Salih, J. C. Knowles, and I. Olsen, "The effect of MgO on the solubility behavior and cell proliferation in a quaternary soluble phosphate based glass system," *J Mater Sci-Mater M*, vol. 13, pp. 549–556, 2002.
- [19] A. J. Parsons, I. Ahmed, C. D. Rudd, G. J. Cuello, E. Pellegrini, D. Richard, *et al.*, "Neutron scattering and ab initio molecular dynamics study of cross-linking in biomedical phosphate glasses," *Journal of Physics: Condensed Matter*, vol. 22, p. 485403, Dec 8 2010.
- [20] G. Walter, J. Vogel, U. Hoppea, and P. Hartmann, "The structure of CaO–Na₂O–MgO–P₂O₅ invert glass," *J Non Cryst Solids*, vol. 296, pp. 212–223, 2001.
- [21] E. Kordes, W. Vogel, and R. Feterowsky, "Physikalisch-chemische Untersuchungen über die Eigenschaften und den Feinbau von Phosphatgläsern," *Zeitschrift für Elektrochemie, Berichte der Bunsengesellschaft für physikalische Chemie*, vol. 57, pp. 282-289, 1953.
- [22] M. R. Sahar and N. Kamaruddin, "The phase equilibrium of binary MgO- and CaO-phosphate glasses," *J Mater Sci Lett*, vol. 15, pp. 1932–1934, 1996.
- [23] G. Walter, U. Hoppe, R. Kranold, and D. Stachel, "Structural characterisation of magnesium phosphate glasses by x-ray diffraction," *Phys Chem Glasses B*, vol. 35, pp. 245-252, 1994.
- [24] S. I. S. Shaharuddin, I. Ahmed, D. Furniss, A. J. Parsons, and C. D. Rudd, "Thermal properties, viscosities and densities of (50-x)Na₂O-(x)CaO-50P₂O₅ glasses," *Glass Technol-Part A*, vol. 53, pp. 245–251, 2012.
- [25] O. V. Mazurin, "Problems of compatibility of the values of glass transition temperatures published in the world literature," *Glass Phys Chem+*, vol. 33, pp. 22-36, 2007.

- [26] N. Sharmin, M. S. Hasan, A. J. Parsons, D. Furniss, C. A. Scotchford, I. Ahmed, *et al.*, "Effect of boron addition on the thermal, degradation, and cytocompatibility properties of phosphate-based glasses," *Biomed Res Int*, vol. 2013, p. 902427, 2013.
- [27] A. B. Seddon, V. K. Tikhomirov, H. Rowe, and D. Furniss, "Temperature dependence of viscosity of Er³⁺-doped oxyfluoride glasses and nano-glass-ceramics," *J Mater Sci-Mater El*, vol. 18, pp. 145-151, 2007.
- [28] J. E. Shelby, "Principles of Glass Formation," in *Introduction to Glass Science and Technology*, J. E. Shelby, Ed., 2 ed Cambridge, UK: The Royal Society of Chemistry, 2005, pp. 7-25.
- [29] A. Inoue, "Amorphous, nanoquasicrystalline and nanocrystalline alloys in Al-based systems," *Prog Mater Sci*, vol. 43, pp. 365-520, 1998.
- [30] M. L. F. Nascimento, L. A. Souza, E. B. Ferreira, and E. D. Zanotto, "Can glass stability parameters infer glass forming ability?," *J Non Cryst Solids*, vol. 351, pp. 3296-3308, 2005.
- [31] A. Hruby, "Evaluation of glass-forming tendency by means of DTA " *Czech J Phys B*, vol. 22, pp. 1187-1193, 1972.
- [32] H. Arstila, E. Vedel, L. Hupa, and M. Hupa, "Factors affecting crystallization of bioactive glasses," *J Eur Ceram Soc*, vol. 27, pp. 1543-1546, 2007.
- [33] S. M. Salman, S. N. Salama, and E. A. Mahdy, "The effect of strontium oxide replacing calcium oxide on the crystallization and thermal expansion properties of Li₂O–CaO–SiO₂ glasses," *Ceram Int*, vol. 41, pp. 137-143, 2015.
- [34] P. Bergo, S. T. Reis, W. M. Pontuschka, J. M. Prison, and C. C. Motta, "Dielectric properties and structural features of barium-iron phosphate glasses," *J Non Cryst Solids*, vol. 336, pp. 159-164, 2004.
- [35] P. Haque, I. Ahmed, A. Parsons, R. Felfel, G. Walker, and C. Rudd, "Degradation properties and microstructural analysis of 40P₂O₅-24MgO-16CaO-16Na₂O-4Fe₂O₃ phosphate glass fibres," *J Non Cryst Solids*, vol. 375, pp. 99-109, 2013.
- [36] D. Muresan, D. Bathory, M. Keul, I. Balasz, and S. Simon, "Local structure and biological effects of vitreous calcium-sodium-phosphate system containing iron," *J Optoelectron Adv M*, vol. 7, pp. 2835 - 2838, 2005.
- [37] M. Lu, F. Wang, Q. Liao, K. Chen, J. Qin, and S. Pan, "FTIR spectra and thermal properties of TiO₂-doped iron phosphate glasses," *J Mol Struct*, vol. 1081, pp. 187-192, 2015.
- [38] B. Qian, S. Yang, X. Liang, Y. Lai, L. Gao, and G. Yin, "Structural and thermal properties of La₂O₃-Fe₂O₃-P₂O₅ glasses," *J Mol Struct*, vol. 1011, pp. 153-157, 2012.
- [39] D. A. Magdas, O. Cozar, V. Chis, I. Ardelean, and N. Vedeanu, "The structural dual role of Fe₂O₃ in some lead-phosphate glasses," *Vib Spectrosc*, vol. 48, pp. 251-254, 2008.
- [40] S. Bruni, F. Cariati, and D. Narducci, "Infrared specular reflection spectra of copper-zinc phosphate glasses," *Vib Spectrosc*, vol. 7, pp. 169-173, 1994.
- [41] N. Sharmin, M. S. Hasan, C. D. Rudd, D. Boyd, U. Werner-Zwanziger, I. Ahmed, *et al.*, "Effect of boron oxide addition on the viscosity-temperature behaviour and structure of phosphate-based glasses," *J Biomed Mater Res B*, Jan 9 2016.
- [42] R. Ciceo-Lucacel, T. Radu, O. Ponta, and V. Simon, "Novel selenium containing boro-phosphate glasses: preparation and structural study," *Materials Science and Engineering C*, vol. 39, pp. 61-6, Jun 1 2014.
- [43] V. Wazer and R. John, *Phosphorus and its compounds*. New York: Interscience Publishers, 1958.
- [44] J. C. Knowles, "Phosphate based glasses for biomedical applications," *J Mater Chem*, vol. 13, p. 2395, 2003.
- [45] L. Koudelka and P. Mošner, "Study of the structure and properties of Pb–Zn borophosphate glasses," *J Non Cryst Solids*, vol. 293-295, pp. 635-641, 2001.

- [46] D. Carta, D. M. Pickup, J. C. Knowles, I. Ahmed, M. E. Smith, and R. J. Newport, "A structural study of sol-gel and melt-quenched phosphate-based glasses," *J Non Cryst Solids*, vol. 353, pp. 1759-1765, 2007.
- [47] N.-J. Kim, S.-H. Im, D.-H. Kim, D.-K. Yoon, and B.-K. Ryu, "Structure and Properties of Borophosphate Glasses," *Electron Mater Lett*, vol. 6, pp. 103-106, 2010.
- [48] M. Elisa, B. A. Sava, A. Diaconu, L. Boroica, D. Ursu, I. Stamatina, *et al.*, "Thermal properties of ecological phosphate and silicate glasses," *Glass Phys Chem+*, vol. 35, pp. 596-601, 2010.
- [49] T. Okura, T. Miyachi, and H. Monma, "Properties and vibrational spectra of magnesium phosphate glasses for nuclear waste immobilization," *J Eur Ceram Soc*, vol. 26, pp. 831-836, 2006.
- [50] D. N. Singh, "Periodic Table and Periodicity of Properties " in *Basic Concept of Inorganic Chemistry* D. N. Singh, Ed., ed India: Pearson Education 2009, pp. 1-32.
- [51] J. Massera, C. Claireaux, T. Lehtonen, J. Tuominen, L. Hupa, and M. Hupa, "Control of the thermal properties of slow bioresorbable glasses by boron addition," *J Non Cryst Solids*, vol. 357, pp. 3623-3630, 2011.
- [52] P. Y. Shih, S. W. Yung, and T. S. Chin, "Thermal and corrosion behavior of P₂O₅-Na₂O-CuO glasses," *J Non Cryst Solids*, vol. 224, pp. 143-152, 1998.
- [53] P. Y. Shih and T. S. Chin, "Preparation of lead-free phosphate glasses with low T_g and excellent chemical durability," *J Mater Sci Lett*, vol. 20, pp. 1811 – 1813, 2001.
- [54] K. Isozaki, H. Hosono, H. Kokumai, H. Kawazoe, T. Kanazawa, and Y. Gohshi, "Co-ordination of Mg²⁺ in MgO-P₂O₅ glasses," *J Mater Sci*, vol. 16, pp. 2318-2319, 1981/08/01 1981.
- [55] P. W. McMillan, *Glass-ceramics*. London, New York: Academic Press, 1979.
- [56] U. B. Chanshetti, V. A. Shelke, S. M. Jadhav, S. G. Shankarwar, T. K. Chondhekar, A. G. Shankarwar, *et al.*, "Density and molar volume studies of phosphate glasses," *Facta universitatis-series: Physics, Chemistry and Technology*, vol. 9, pp. 29-36, 2011.
- [57] M. S. Hasan, I. Ahmed, A. J. Parsons, G. S. Walker, and C. A. Scotchford, "Material characterisation and cytocompatibility assessment of quinary phosphate glasses," *J Mater Sci-Mater M*, vol. 23, pp. 2531-41, Oct 2012.